Force sensing and transmission in human induced pluripotent stem-cell-derived pericytes

Iendaltseva, O.

Chapter 2

Towards capillary basement membrane *in vitro* modeling [1]

abstract

Basement membranes (BMs) represent thin layers of compact, spatially organized extracellular matrix (ECM) proteins that surround most tissues, and align epithelium and vascular endothelium in the body. *In vitro* reconstruction of any organ or tissue that comprises BMs, requires either inclusion of single ECM proteins, formation of the BM ECM scaffold, or development of a system resembling BM functions. Here, we focused on modeling of the capillary BM part that acts as a mediator of mechanical interaction between pericytes (PC) and endothelial cells (ECs). By using 2D ECM modeling techniques, such as protein microcontact printing (μCP) onto surfaces of different stiffness we could mimic the capillary BM rigidity range and unique spatial organization of two main ECM components – laminin (LM)-411/511 and fibronectin (FN). Our system is useful for studying interactions in the PC-EC interstitial layer of the capillary BM and can be expanded to the complete capillary BM model by adding the collagen-rich second layer.

1. This chapter is based on: O. Iendaltseva, V.V. Orlova, C.L. Mummery, E. H. J. Danen and T. Schmidt, Fibronectin Patches as Anchoring Points for Force Sensing and Transmission in Human Induced Pluripotent Stem Cell-Derived Pericytes, published in *Stem Cell Reports*, 2020

2.1 Introduction

Biochemical and spatial organization of extracellular matrix (ECM) proteins, as well as, matrix stiffness have implications for cell behavior [1–3]. It is important to combine all these factors in order to accurately reproduce the cell microenvironment *in vitro*. The capillary basement membrane(BM) has a unique organization of its three main components – collagen IV, laminin-411/511 and fibronectin that are used for attachment of cells in the capillary wall [4–7]. Endothelial cells attach mainly to laminin, for pericytes this is less well understood. Here ,we revised existing approaches in ECM modeling to develop an *in vitro* model of the BM that can be used to study the biochemical and mechanical interaction of vessel cells such as endothelial cells and pericytes with the BM.

There are many properties of a cell's physical environment that can be mimicked to study their influence on the cell's behavior. These include the biochemical composition, stiffness and geometry of the surrounding ECM. In addition, tissue-level mechanical signals such as tissue rigidity that depends on cell density and intercellular forces, or aspects such as shear stress or hydrostatic pressure in blood vessels, or dynamic mechanical loads such the beating heart [3].

Approaches to mimic ECM protein composition and stiffness of different tissues include 2D and 3D substrates and can be roughly divided into four major categories: decellularized matrices, nanofibrous scaffolds, biomimicking gels and arrays of micro- and nano-posts (Table. 2.1) [20]. Here we will briefly describe the main principles.

Tissue decellularization allows obtaining a natural, cell-assembled matrix, which includes all tissue-specific ECM components in a physiologically correct arrangement that cannot be reached by using just pure proteins or synthetic materials [8]. However, composition of such matrices, as well as their stiffness, is not fully known and varies from donor to donor, restricting their usefulness as a preclinical model.

Nanofiber fabrication [9] is focused on the use of only essential ECM components such as collagen, laminin, fibronectin and other fibrous proteins. These proteins can be used directly to create nanofibrous scaffolds or blended with synthetic (usually biodegradable) polymers to compensate for their rapid degradation and low mechanical strength. Electrospinning [10], phase separation [11], self-assembly [12] and other techniques were developed to obtain 2D or 3D nanofibrous scaffolds with a set

Category	Dimen-tions	Strengths	Limitations	Referen-ces
Decellularized matrices	3D	Natural, cell-assembled matrix. Includes all tissue-specific ECM components in a correct arrangement	Composition and mechanical properties are not fully known and vary from donor to donor	[8]
Nanofibrous scaffolds	2D, 3D	ECM scaffolds with defined protein composition, fiber diameter, alignment, length and crosslinking density. Allows obtaining scaffolds of different stiffness	Impossibility to fine tune the spatial organization of ECM proteins. Nanofiber scaffold stiffness dependence on its protein composition and density	[9–12]
Biomimicking gels	2D, 3D	Decouple the effect of ECM stiffness from it's biochemical composition; cell TFM	Gel porosity, which depends on concentration of crosslinker, showing increase in the pore size with decrease in the gel stiffness	[13–16]
Arrays of micro- and nano-posts	2D, 3D	TFM on substrates of different rigidity, independently from substrates-coupled ECM feedback	3D geometry of the array surface or restricted, by the post diameter, cell FAs size	[17–19]

Table 2.1: ECM mimicking approaches

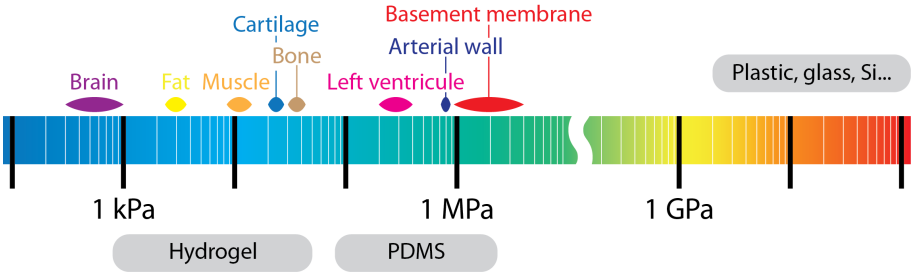

Figure 2.1: Biological rigidity range

fiber diameter, length and crosslinking density that ultimately define the scaffold's resulting stiffness. The main limitations of this approach are the impossibility to fine-tune the spatial organization of ECM proteins and the dependence of the scaffold stiffness on its protein composition and density.

ECM proteins can also be coated on synthetic polymer gels of a certain stiffness to decouple the effect of the biochemical composition and protein density from the matrix stiffness. Polyacrylamide (PAA) [13], hydroxy-polyacrylamide (hPAA)[14] and polydimethylsiloxane (PDMS) [15] gels suit well and are widely used as biomimicking gels for 2D setups. Adding a defined volume of crosslinker while keeping the amount of base polymer unchanged allows to control the rigidity of such gels. PAA and hPAA hydrogels can be prepared in the stiffness range starting from 0.1 kPA, while PDMS gels are mostly used for the higher stiffness like 100 kPA – 1 MPa. Combined use of such polymers embraces the biologically relevant rigidity range of ∼50 Pa – ∼4 GPa (Fig.2.1). Blending marker beads into these gels also allows performing cell traction force microscopy (TFM) [16]. The drawback of such an approach is gel porosity, which depends on the concentration of crosslinker, showing an increase in the pore size with a decrease in the gel stiffness. This influences mechanical feedback from the substrate-coupled ECM in addition to the change in total bulk stiffness of the gel [21].

As an alternative, arrays of Silicone (Si)/PDMS nano- [17, 18] or PDMS micro- [19] posts can be used to measure cell traction forces on substrates of different rigidity, independently from substrate-coupled ECM feedback. Changing the geometry of the posts, but not the amount of crosslinker in the polymer, controls the stiffness of such arrays. Longer posts yield lower rigidity. ECM proteins can be coated on top of the

posts or in between them, depending on the experiment goal, and the rest of the surface is passivated to prevent unspecific cell binding. Nevertheless, this system also has some disadvantages like 3D geometry of the array surface or the restricted cell-ECM attachment area due to the small diameter of the individual posts.

Taken together, all existing systems have their advantages and disadvantages and the experimental approach should be carefully chosen, depending on the cellular process of interest and effects that can be neglected.

As aforementioned, ECM matrix has not only certain mechanical properties and biochemical composition, but in many cases, also a defined spatial organization of proteins. For instance, in the vessel BM, laminin and collagen – it's main components – are not mixed , but located in layers [22]. On the other hand, fibronectin in the BM is located in small patches. To mimic such organiztion, placing proteins in a pattern on top of 2D substrates can serve as a scaffold or a guide for cell shaping and alignment [23].

While micro-scale substrate patterning can shape cells, nano-scale patterning can spatially control subcellular structures. For instance, nano-patterning ECM allows to control the distance between individual ECM-binding receptors such as integrins. This, in turn, affects cell substrate adhesion formation, cell spreading area, and cell proliferation [24].

By combining controlled substrate stiffness and spatial organization of proteins, the various aspects of the BM can be mimicked. Here, we are mainly interested in the impact of the ECM at the cellular scale (i.e. not the nano-scale), and we focus on micro-scale patterning techniques.

Microcontact printing (μCP) was first introduced by George M. Whitesides and Amit Kumar in 1993 [25]. Initially it was developed to obtain patterns of self-assembled monolayers (SAM) on top of a gold film, which with a subsequent selective etching would yield well-defined micrometer sized features of gold. At the base of the technique was an elastomer stamp containing a desired pattern surface texture, covered with SAM and pressed onto a Si wafer with a film of gold on it. This resulted in a transferred pattern of SAM on top of the gold film in places were the surface of gold came in contact with the prominent parts of the stamp. The Si wafer was then etched to produce the desired features. The main advantage of this method was a fast production of gold patterns without clean room or photolithographic equipment.

Further, this principle was adopted for cell biology studies to create patterns of ECM proteins on top of different substrates [23, 26, 27]. In the most utilized approach, an elastomer stamp (mainly made of PDMS) would be covered by a protein of interest and then used to "print" a protein micropattern on top of the activated substrate like PDMS gels, Si wafers, glass, polystyrene dishes or PDMS micropillar arrays of a controlled stiffness [28].

To solve some major problems of μCP, when printing of small, far scattered forms is required, a "stamp-off" method was first applied in the group of Christopher Chen [29]. This method represents an extension of the conventional μCP technique. The difference with convenstional μCP is that the PDMS stamp carrying a patterned surface texture, rather than adding a protein layer to a surface, now is used to remove proteins from the flat surface covered with a protein monolayer at places of contact. This leaves the protein only at areas untouched by the PDMS stamp.

Here, we have combined conventional and stamp-off μCP with PDMS- and hPAA-based substrates of controlled stiffness, to mimic the capillary BM ECM composition, spatial organization, and mechanical properties. The models can be used to study the biochemical and mechanical interaction of vascular cells such as endothelial cells and pericytes with the BM.

2.2 Methods

2.2.1 Generation of PDMS flat substrates

PDMS flat substrates were preparead as following. 20g of PDMS elastomer was mixed in the 1:10 crosslinker:prepolymer ratio, degassed for 1h at 150 pressure and spread onto silanized Si blank wafer. This wafer with PDMS on it was degassed again for 15' and curred at 65°C for 16 hours. After polymerization, PDMS was detached from the Si wafer and cut into 10×10 mm pieces.

2.2.2 Patterning of PDMS flat substrates

PDMS micropillar arrays for stamping were prepared as was described before [30] [31]. Briefly, SI mold was made by two-step Deep Reactive Ion Etching (DRIE) process. This yielded a 10×10 mm hexagonal

array of 2 μm diameter holes with 2 μm spacing and varying depth, flanked by two 50 μm deep 10×2 mm tranches. After mold passivation with trichloro silane (Sigma), PDMS 1:10 was poured over it and cured for 20 hours at 110°C. The peeled off PDMS had a negative of the mold shape with micropillar array and 50 μm spacers on the sides. 50 μm spacers were further cut off to ensure a good contact between the flat surface and pillar array.

A FN-dot pattern on top of PDMS substrates was obtained by using a "microcontact printing" method. First, flat PDMS (Sylgard 184,Dow Corning) 1:30 (crosslinker:prepolymer ratio, cured 16 hours at 65°C) stamps were incubated 60' with a 40 μl drop of 50 μg/ml FN plus 10 μg/ml Alexa405-FN in milliQ, washed ones in milliQ and dried under laminar flow. Then, aforementioned PDMS (Sylgard 184,Dow Corning) 1:10 (crosslinker:prepolymer ratio, cured 20 hours at 110°C) micropillar arrays with spacers cut off were 10' UV-ozone activated and inverted on top of the PDMS stamp for 10'. Further, micropillar arrays with FN on them were pressed onto the UV-ozone activated PDMS substrates surface for 10'. Before removing PDMS micropillar arrays, everything was immersed with 100% Ethanol. After PDMS micropillar arrays were gently detached from the PDMS substrates, 100% Ethanol was replaced, first, with 70% Ethanol and then with 1% BSA 60'at room temperature to block the rest of the surface.

A grid of crossing FN and LM lines pattern on top of the PDMS substrates was obtained by combining "stamp-off" and "microcontact printing" methods [32]. First, two PDMS 1:10 molds with 5 μm high lines of different width were produced by using replica-molding from a silicon wafer. After UV-ozone activation 10', they were pushed onto PDMS 1:30 stamps with a protein layer dried on them. Followed by 10' incubation and removal, this molds left a negative of the pattern in the protein layer on top of the PDMS stamps. Further, PDMS stamps were inverted on top of the UV-ozone activated PDMS 1:10 surface, creating a pattern of crossing LM and FN lines on it (Fig. 2.3a). As a last step, everything was immersed with 100% Ethanol, then 100% Ethanol was replaced, first, with 70% Ethanol and then with 1% BSA for 60' at room temperature to block the rest of the suface.

A pattern on top of PDMS flat 1:10 (crosslinker:prepolymer ratio, cured 16 hours at 65°C) substrates, where LM would surround FN spots or the inverse organization, was produced by combining "stamp-off" and

"microcontact printing" methods [32]. Two flat PDMS (Sylgard 184,Dow Corning) 1:30 (crosslinker:prepolymer ratio, cured 16 hours at 65°C) stamps were separately incubated for 60' with LM-111 (Sigma, l2020) and mixture of Alexa405-labeled and unlabeled FN (Sigma, f1141), washed with milliQ and dried under laminar flow. With a help of UV-ozone activated PDMS 1:10 micropillar arrays, were obtained holes in one of the layers. Further, two stamps were inverted one by one on top of the UV-ozone activated PDMS 1:10 surface and incubated for 10' each, to get previously modified protein sheet on top of the uninterrupted layer of – second (Fig. 2.2a, b).

PDMS surfaces with FN lines under a layer of LM with holes were printed by using PDMS stamps with LM and FN layers modified as aforementioned. A PDMS micropillar array was used to make holes in the dry LM monolayer and PDMS mold with lines – to create a line pattern in FN. Further, this stamps were loaded for 10' each on top of the UV-ozone activated PDMS surface, with FN stamp going first (Fig. 2.3b). Finally, all patterned PDMS surfaces were washed with 100% Ethanol, followed by 70% Ethanol and blocked by using 1% BSA 60'.

2.2.3 Generation of hPAA hydrogel

hPAAm hydrogels were made following a previously described method [14]. Gels stiffer then 40 kPa were obtained following the same procedure as suggested in [33] and [34] by increasing polyacrylamide mono-mer concentration with a fixed monomer/crosslinker ratio of 29:1.

2.2.4 Generation of PDMS gel

PDMS gels were generated similar to the procedure described before. First, 13 mm glass coverslips were cleaned in milliQ and ethanol, dried and treated 10' in the UV-ozone chamber. Then, PDMS (Sylgard 184, Dow Corning) prepolymer was mixed with the crossliker in different ratios from 10:1 to 100:1, degasssed and spread on top of the glass coverslips, followed by curring at 65°C for 16 hours.

2.2.5 hPAA hydrogel and PDMS gel patterning

A pattern on top of hPAA hydrogels and PDMS gels, where LM would surround FN spots was produced by combining "stamp-off" and

"microcontact printing" methods [32]. First, stamps were prepared in the same way for both types of gels. A 40 µl drop of 50 µg/ml LM-111 in milliQ water was incubated for 60' on top of the 10 × 10 mm PDMS (Sylgard 184,Dow Corning) 1:30 (crosslinker:prepolymer ratio, cured 16 hours at 65°C) stamp, followed by washing and drying under laminar flow. Then OV-ozone activated PDMS micropillar array was pushed onto the dry LM-111 monolayer to obtain holes in the places of micropillar-LM-111 contacts. After 10' incubation the array was removed and a second 40 µl drop of 50 µg/ml FN plus 10 µg/ml Alexa405-FN in milliQ was gently spread onto the first layer for 60'. Finally, the stamp was washed and dried under laminar flow.

Hydroxy-PAAm hydrogels were dried using nitrogen flow and incubated with the stamp for 60' (Fig. 2.6a), following blocking with 1% BSA in PBS o/n and washing with PBS.

PDMS gels were 8' OV-ozone activated and incubated with a stamp for 10', following blocking with 1% BSA in PBS or 0.2% Pluronic (F-127, Sigma) in PBS for 60' and washing with PBS.

2.2.6 hPAA hydrogel and PDMS gel imaging

Confocal imaging was performed on a home-built setup based on an Axiovert200 microscope body (Zeiss), spinning disk unit (CSU-X1, Yokogawa) and an emCCD camera (iXon 897, Andor). IQ-software enabled setup-control and data acquisition. Lasers of 405 nm (CrystaLaser), 488 nm (Coherent), 514 nm, 561 nm (Cobolt) and 642 nm (Spectra Physics) wavelength were coupled into the CSU via polarization maintaining single-mode fiber. For PDMS and hPAA 2D assays parafilm spacers were made directly on top of the glass coverslips.This approach ensured reproducible cell observation within the limited working distance of a high-NA objective on an inverted microscope.

2.3 Results

2.3.1 PDMS surface micropatterning

First, to generate a pattern of micron sized spots of FN on a flat surface, which would resemble FN deposits in the capillary BM, we used PDMS micropillar arrays as a stamp for FN dots and several test substrates following microcontact printing technique. Test substrates included PDMS flat surface prepared in the ratio 1:10 crosslinker:base and cured in a polystyrene dish, PDMS flat surface 1:10 cured on a Si blank wafer and glass coverslips. PDMS micropillars had 2 μm diameter, hexagonal order and 2 μm spacing. Stamping was tested using pillar arrays of two different stiffness – 47.2 kPA and 137 kPa. After test surfaces were cleaned and activeted with UV-ozone, micropillar arrays having FN on top of the pillars were pressed into them. Alexa647 FN labeling prior to experiment allowed to examine stamping results with confocal microscope (Supplementary Fig. 2.7). Stamping a PDMS flat surface prepared on a blank Si wafer with 137 kPa stiff micropillar array yielded the most homogeneous and reproducible pattern of FN dots (Supplementary Fig. 2.7e) and this combination was chosen for further experiments. Next, we tested two surface passivation ways to prevent unspecific binding of cells. Stamped PDMS surfaces were incubated for 1 hour with either 1%BSA in PBS or 0.2%Pluronic in PBS, washed and seeded with cells. After 4 hours incubation cells were fixed, stained for F-actin and the average cell spreading area was determined (Supplementary Fig. 2.8). Both approaches showed effective passivation with no difference in effect on cell spreading behavior.

To further introduce LM into the system, a PDMS suface patterned with FN dots was coated or stamped with a thin layer of LM-111 or matrigel. Cells readily attached to substrates, but were not able to sense FN dots (data not shown). To solve this issue a reverse approach was taken. Following "stamp-off" method principles, a PDMS micropillar array was used to make holes in the LM layer, which was further transferred onto a PDMS flat surface stamped with a FN monolayer (Fig. 2.2a). This approach yielded a pattern were FN was exposed through hexagonally ordered 2 μm wide holes in the LM layer (Fig. 2.2c). For the cell adhesion assays an inverse pattern was additionally generated (Fig. 2.2d) where LM was exposed through holes in a FN layer (Fig. 2.2b). Besides this, a pattern of crossing LM and FN lines (Fig. 2.3a, 2.3c) together

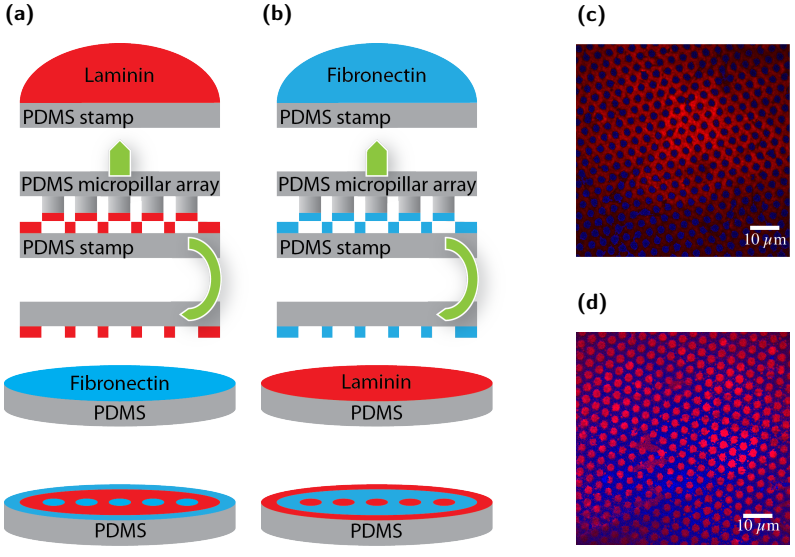

Figure 2.2: (a and b) "micro contact printing" schemes for patterns with: (c) FN spots surrounded by LM-111, (d) LM-111 spots surrounded by FN

with FN lines exposed through holes in LM layer (Fig. 2.3b, 2.3d) were developed using microcontact printing and "stamp-off" techniques.

To investigate whether gel stiffness influences precision of the gel surface patterning and accuracy of patterned features, a pattern steepness was assessed for PDMS and hPAA gels of different rigidity. Pattern steepness of the LM layer with holes and FN/LM lines was determined from an intensity profile (Fig. 2.4). The intensity profile (Fig. 2.4b) was read from the cross section set manually by the line (Fig. 2.4a) and a distance from the 20% peak hight and 80% was determined as pattern steepness Δx (Fig. 2.4b). Pattern containing microholes showed higher steepness than FN/LM crossing lines (Fig. 2.5).

2.3.2 PDMS gels micropatterning

Subsequently, to introduce stiffness into our model we generated PDMS gels of different rigidities by varying the base:crosslinker ratio according to a technology described earlier [21]. Base:crosslinker ratios were taken from 1:10 to 1:100 yielding PDMS gels in a ~2300 kPa –

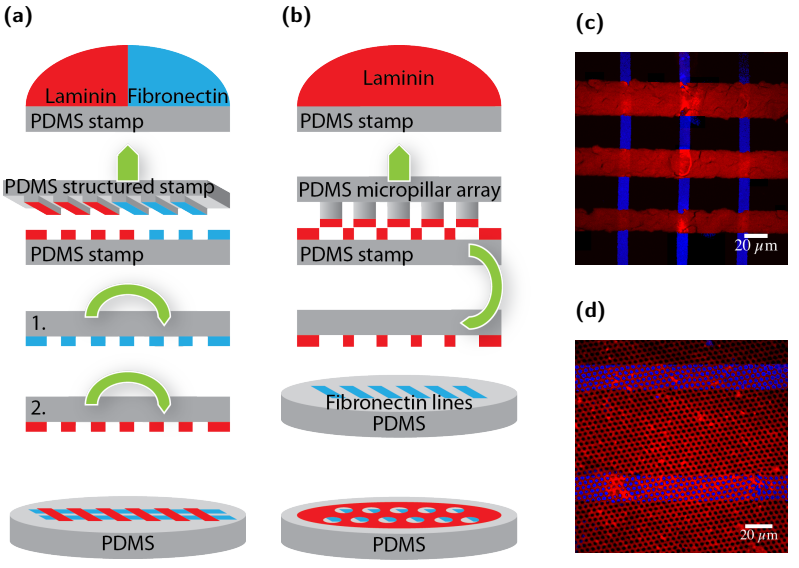

Figure 2.3: (a – b) "micro contact printing" schemes for patterns with: (c) a grid of crossing LM-111 and FN lines, (d). FN lines stamped under a layer of LM-111 with holes.

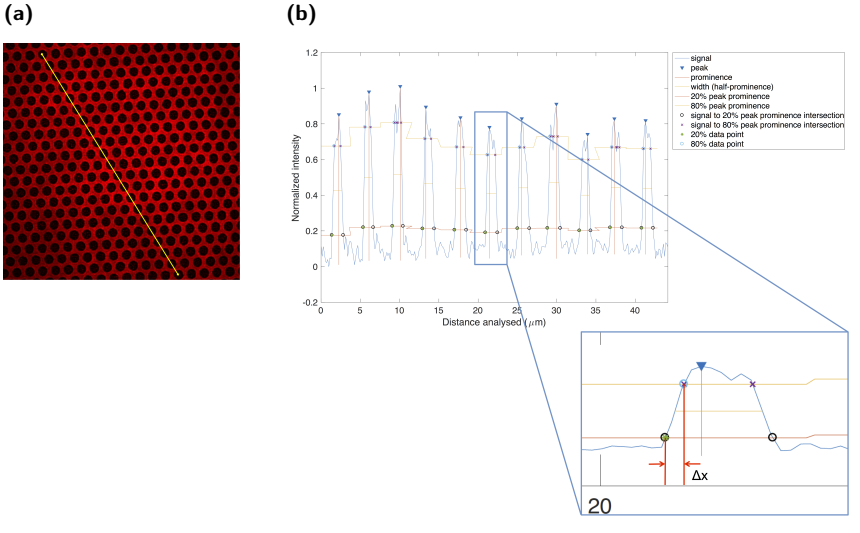

Figure 2.4: Determining pattern steepness. (a) Manually set with a line cross section of intensity profile. (b) Pattern intensity profile and magnified image of the peak steepness Δx detection on 20% and 80% height

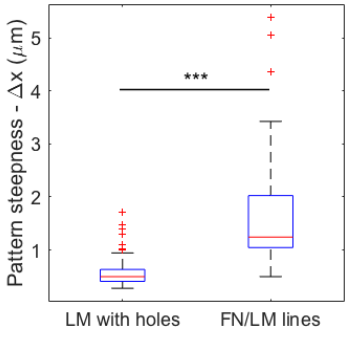

Figure 2.5: LM with holes and FN/LM crossing line pattern steepness on PDMS, determined from the intensity profile. NS, P>0.05; *P<0.05; **P<0.005; ***P<0.0005 according to Mann - Whitney test

0.1 kPa stiffness range accordingly. However gel exposure to UV-ozone enabling protein binding resulted in surface wrinkling for gels with rigidities below 40 kPa. Such an effect can be explained by the formation of a silica (SiO_2)-like stiffer layer on the PDMS surface caused by the formation of new Si-O-Si bonds under plasma oxidation [35, 36]. By decreasing the time of UV-ozone treatment from 10 min to 5 min we could prevent wrinkle formation, but surface patterning became impossible due to stickyness of the gel caused by insufficient crosslinking.

2.3.3 hPAA gels micropatterning

As an alternative, we used hPAA hydrogels that were reported to provide the same flexibility in substrate micropatterning as PDMS gels, but remain polyacrylamide hydrogel precision in controlling stiffness [14]. Authors utilized this method to obtain pattern structures $> 10\ \mu m$ in size, while our FN spots required to go down to $2\ \mu m$ scale.

First, we tested two stamping approaches that as aforementioned showed good results for PDMS flat surface stamping: i)direct patterning with micropillar arrays of 137 kPa stiffness and ii) two step stamping of FN monolayer with hole patterned LM layer on top (Fig. 2.2a). The first approach appeared to be not suitable due to the uneven surface of the gel, which did not allow to obtain sharp, homogeneous patterns of the dots on top of the gel surface (Supplementary Fig. 2.9a). Furthermore, stiff thin pillars would create micropits in the gel surface under certain

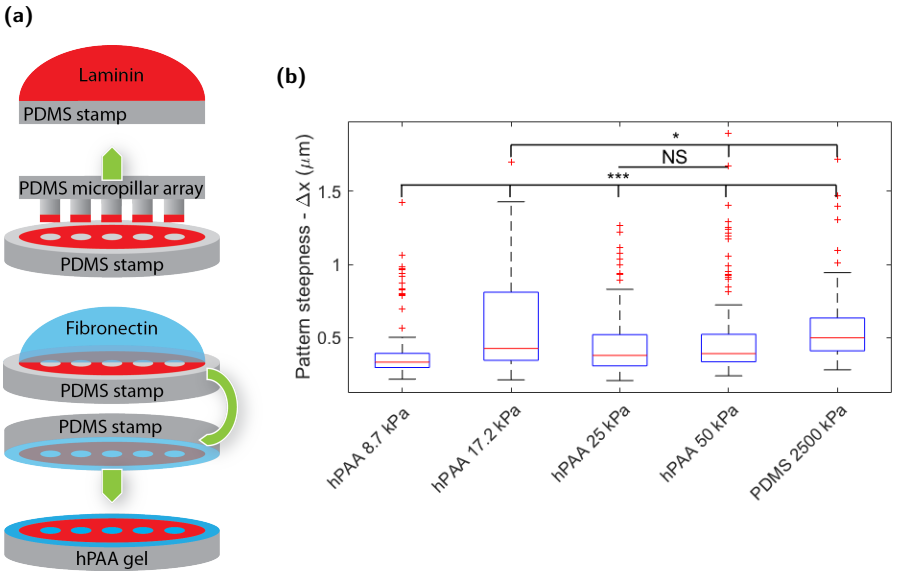

Figure 2.6: hPAA hydrogels patterning. (a) "micro contact printing" scheme for hPAAm hydrogels with FN spots surrounded by LM-111. (b) Pattern steepness on hPAA gels of several stiffness compared to the one on PDMS flat surface. NS, P>0.05; *P<0.05; **P<0.005; ***P<0.0005 according to Mann - Whitney test

pressure on the micropillar array stamp. In the second case we discovered that the LM layer simply didn't bind on top of FN to the surface of the gel (Supplementary Fig. 2.9b).

To obtain a desirable pattern of FN dots surrounded by LM on top of the hPAA hydrogels we developed an approach based on the technique mentioned in [29]. In this paper authors used "re-inking" of the PDMS stamp after modification of the first protein layer via "stamp-off" approach. Hence, in our new microcontact printing sequence a PDMS stamp was first covered by LM-111, then the UV-ozone activated PDMS micropillar array was pressed into the dried LM layer to create holes in it, followed by PDMS stamp "re-inking" with FN, drying and inverting onto the dried hPAA gel for 1 hour. The resulting pattern resembled the earlier obtained on top of the flat PDMS surface (2.2c) and had good reproducibility. Pattern sharpness quantification showed steepness values within 1 μm for layer of LM with holes on top of hPAA gels of different stiffness (Fig. 2.6b)

2.4 Discussion

BMs are spatially organized into a thin sheet of ECM underlying every epithelium and vascular endothelium [37–39], mainly built from collagen type IV, LM and proteoglycans. Although BMs are extensively studied, their *in vitro* mimicking is challenging and commonly limited to 2D coating to replicate the BM biochemical composition, ECM protein functionalization of gels or micro/nano post arrays to resemble the BM mechanical properties or designs that allow investigating the BM functionality, like PDMS porous thin films or nanofibrous scaffolds [40–42]. Recent findings revealed that LM and type IV collagen are not organized into one homogeneous network, but form two layers, allowing fibroblasts to interact with collagen on one side and epthelial cells or EC to interact with LM on the other [22]. Moreover, deposits of FN are found by EM in the LM-rich layer in vivo [4, 7, 43]. Here, we focussed on designing an *in vitro* model of the PC-EC interaction environment of the capilarry BM (Fig. 1.1).

The BM itself is on average 200-400 nm thick [44, 45] and requires 3D ECM modeling, while the PC-EC interstitial layer is much thinner and allowed us to use 2D ECM modeling approaches, such as protein μCP on top of substrates of controlled rigidity. This approach was chosen to mimic LM and FN spatial organization in the BM and its overall stiffness. Our first attempt to obtain FN dots on top of PDMS gels of different stiffness, prepared according to the protocol used in [21], revealed unwanted wrinkle formation on the gel surfaces with stiffness lower 40 kPa after exposure to the UV-ozone. This effect has been shown by other studies [35, 36] to be related to the stiffer silica (SiO_2)-like layer formation on the PDMS surface under UV-ozone treatment. While on stiff PDMS gels this effect is not directly visible, on the soft ones it results in surface wrinkling. Although such a phenomenon is extensively used to obtain PDMS surfaces with grooves of a controlled geometry [46–48], for our model it is not acceptable, making the stiffness of PDMS gels unreliable.

We observe that μCP on top of hPAA hydrogels represents a better system in comparison to μCP on PDMS gels, to obtain spatially organized proteins on top of matrices of low stiffness in a range that is biologically relevant for microvessels [49, 50]. The presence of N-hydroxyethylacrylami-de (HEA) in these gels results in a constant availability of hydroxyl groups on the gel surface enabling hydrogen protein

bonding without the need of surface hydroxylation with oxygen plasma, piranha, HF, UV-ozone etc., as is needed in case of glass, Si or PDMS substrates [51]. We also find that the size of μCP pattern features can be lowered from $> 10\ \mu m$ to $2\ \mu m$ by combining hPAA gels with a "stamp-off" protein printing approach that previously was mainly used for micropatterning on a PDMS flat surface or PDMS micropillar arrays. Importantly, pattern steepness on hPAA hydrogels is not lower than the one on PDMS flat surface and does not depend on the gel stiffness. A possible explanation for the last observation is that hPAA gel stamping is preceeded by dehydration of the gel μCP and followed by gel rehydration when stamping is finished. Hence, at the moment of protein printing all gels have highly similar stiffnesses allowing for identical pattern qualities. This makes our system easy to reproduce and use.

Taken together, our model represents the PC-EC interstitial layer of the capillary BM, including the LM layer and the FN deposits. Our combinations of stamping approaches will be of general applicability to create heterogenous patterned surfaces resembling other biological structures. The combination of stamping techniques and hydrogels of variable stiffness allows investigating responses of cells to altered substrate stiffness. Our design does not include analysis of the inverse process: cellular forces applied to the BM. This can be made possible for instance by adding marker beads for traction force microscopy [16]. In addition, our model can be further expanded to represent the complete capillary BM by including proteogycans and adding a seperate layer rich in type IV collagen.

2.5 Appendix

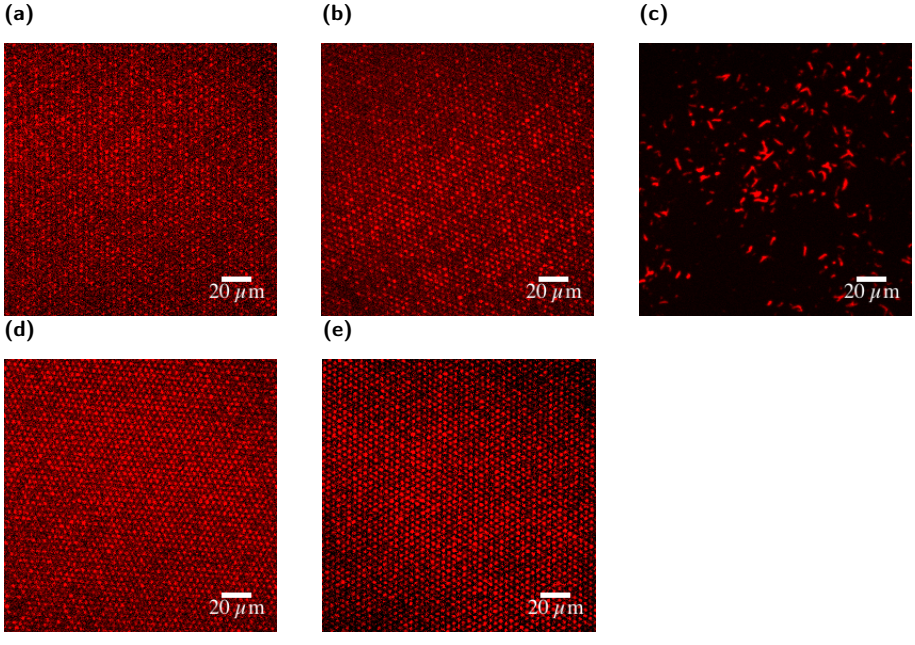

Figure 2.7: FN dots stamping test on top of (a, d) PDMS 1:10 prepared in a polystyrene dish; (b, e) PDMS 1:10 prepared on a Si blank wafer and (c) glass coverslip. Stapming was done with PDMS micropillar arrays of 42.7 kPa (a-c) and 137 kPa (d, e) stiffness

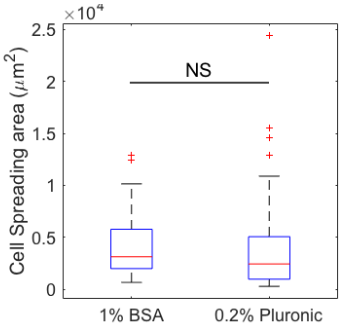

Figure 2.8: Pericyte (CD31-(Dif31) cell line) spreading area after 4 hours incubation on PDMS flat surface stamped with FN dots and blocked with 1% BSA or 0.2% Pluronic. NS, P>0.05; *P<0.05; **P<0.005; ***P<0.0005 according to Mann - Whitney test

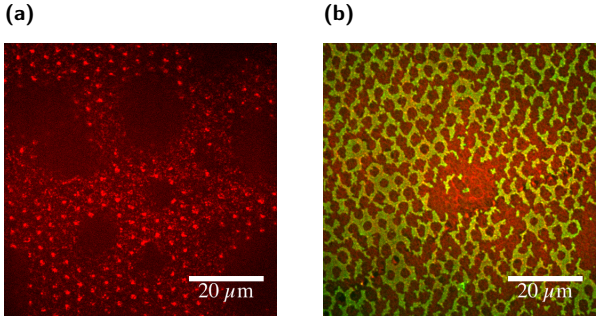

Figure 2.9: FN (red) and LM (green) pattern stamping results on top of the hPAA gels, obtained with PDMS micropillar arrays (a) and "stamp-off" double step protein μCP (b)

Bibliography

[1] Richard O Hynes. « The extracellular matrix: not just pretty fibrils ». In: *Science* 326.5957 (2009), pp. 1216–1219.

[2] Fiona M Watt and Wilhelm TS Huck. « Role of the extracellular matrix in regulating stem cell fate. » In: *Nature Reviews* 14.8 (2013), pp. 467–73. ISSN: 1471-0072.

[3] Christian Frantz, Kathleen M Stewart and Valerie M Weaver. « The extracellular matrix at a glance. » In: *J. Cell. Sci.* 123.Pt 24 (2010), pp. 4195–200. ISSN: 0021-9533.

[4] Annika Armulik, Alexandra Abramsson and Christer Betsholtz. « Endothelial-pericyte interactions. » In: *Circ. Res.* 97.6 (2005), pp. 512–23. ISSN: 0009-7330.

[5] Raghu Kalluri. « Basement membranes: structure, assembly and role in tumour angiogenesis ». In: *Nature Reviews Cancer* 3.6 (2003), pp. 422–433. ISSN: 1474-175X.

[6] Rupert Hallmann et al. « Expression and Function of Laminins in the Embryonic and Mature Vasculature ». In: *Physiol Rev.* 85.3 (2005), pp. 979–1000. ISSN: 0031-9333.

[7] PJ Courtoy and J Boyles. « Fibronectin in the microvasculature: localization in the pericyte-endothelial interstitium. » In: *J. Ultrastruct. Res.* 83.3 (1983), pp. 258–73. ISSN: 0022-5320.

[8] Greg M Harris, Irene Raitman and Jean E Schwarzbauer. « Cell-derived decellularized extracellular matrices. » In: *Methods Cell Biol.* 143 (2018), pp. 97–114. ISSN: 0091-679X.

[9] Rajesh Vasita and Dhirendra S Katti. « Nanofibers and their applications in tissue engineering. » In: *Int J Nanomedicine* 1.1 (2006), pp. 15–30. ISSN: 1176-9114.

[10] Quynh P Pham, Upma Sharma and Antonios G Mikos. « Electrospinning of polymeric nanofibers for tissue engineering applications: a review. » In: *Tissue Eng.* 12.5 (2006), pp. 1197–211. ISSN: 1076-3279.

[11] PX Ma and R Zhang. « Synthetic nano-scale fibrous extracellular matrix. » In: *J. Biomed. Mater. Res.* 46.1 (1999), pp. 60–72. ISSN: 0021-9304.

[12] Peter Berndt, Gregg B Fields and Matthew Tirrell. « Synthetic lipidation of peptides and amino acids: monolayer structure and properties. » In: *Journal of the American Chemical Society* 117.37 (1995), pp. 9515–9522. ISSN: 0002-7863.

[13] RJ Pelham and Yl Wang. « Cell locomotion and focal adhesions are regulated by substrate flexibility. » In: *Proc. Natl. Acad. Sci. U.S.A.* 94.25 (1997), pp. 13661–5. ISSN: 0027-8424.

[14] Thomas Grevesse et al. « A simple route to functionalize polyacrylamide hydrogels for the independent tuning of mechanotransduction cues. » In: *Lab on a Chip* 13.5 (2013), pp. 777–80. ISSN: 1473-0189.

[15] Rachelle N Palchesko et al. « Development of Polydimethylsiloxane Substrates with Tunable Elastic Modulus to Study Cell Mechanobiology in Muscle and Nerve ». In: *PLoS ONE* 7.12 (2012).

[16] Ulrich Schwarz and Jérôme Soiné. « Traction force microscopy on soft elastic substrates: A guide to recent computational advances ». In: *Biochimica Et Biophysica Acta Bba - Mol Cell Res* 1853.11 (2015), pp. 3095–3104. ISSN: 0167-4889.

[17] Zhou Li et al. « Quantifying the traction force of a single cell by aligned silicon nanowire array. » In: *Nano Lett.* 9.10 (2009), pp. 3575–80. ISSN: 1530-6984.

[18] Jau-Ye Shiu et al. « Nanopillar force measurements reveal actin-cap-mediated YAP mechanotransduction ». In: *Nat Cell Biol* 20.3 (2018), pp. 262–271. ISSN: 1465-7392.

[19] John L Tan et al. « Cells lying on a bed of microneedles: an approach to isolate mechanical force. » In: *Proc. Natl. Acad. Sci. U.S.A.* 100.4 (2003), pp. 1484–9. ISSN: 0027-8424.

[20] Dhwani Jhala and Rajesh Vasita. « A Review on Extracellular Matrix Mimicking Strategies for an Artificial Stem Cell Niche ». In: *Polymer Reviews* 55.4 (2015), pp. 561–595. ISSN: 1558-3724.

[21] Britta Trappmann et al. « Extracellular-matrix tethering regulates stem-cell fate. » In: *Nat Mater* 11.7 (2012), pp. 642–9. ISSN: 1476-1122.

[22] Willi Halfter et al. « The bi-functional organization of human basement membranes. » In: *PLoS ONE* 8.7 (2013), e67660. ISSN: 1932-6203.

[23] R Singhvi et al. « Engineering cell shape and function ». In: *Science* (1994). ISSN: 0036-8075.

[24] Jinghuan Huang et al. « Impact of order and disorder in RGD nanopatterns on cell adhesion. » In: *Nano Lett.* 9.3 (2009), pp. 1111–6. ISSN: 1530-6984.

[25] Amit Kumar and George M Whitesides. « Features of gold having micrometer to centimeter dimensions can be formed through a combination of stamping with an elastomeric stamp and an alkanethiol "ink" followed by chemical etching ». In: *Appl Phys Lett* 63.14 (1993), pp. 2002–2004. ISSN: 0003-6951.

[26] A Bernard et al. « Printing patterns of proteins ». In: *Langmuir* (1998). ISSN: 0743-7463.

[27] CD James et al. « Patterned protein layers on solid substrates by thin stamp microcontact printing ». In: *Langmuir* (1998). ISSN: 0743-7463.

[28] John L Tan et al. « Simple Approach to Micropattern Cells on Common Culture Substrates by Tuning Substrate Wettability ». In: *Tissue Eng* 10.5-6 (2004), pp. 865–872. ISSN: 1076-3279.

[29] Ravi A Desai et al. « Subcellular spatial segregation of integrin subtypes by patterned multicomponent surfaces. » In: *Integr Biol (Camb)* 3.5 (2011), pp. 560–7. ISSN: 1757-9694.

[30] Hedde van Hoorn et al. « The Nanoscale Architecture of Force-Bearing Focal Adhesions ». In: *Nano letters* 14 (2014), pp. 4257–4262.

[31] Olivia du Roure et al. « Force mapping in epithelial cell migration. » In: *Proc. Natl. Acad. Sci. U.S.A.* 102.7 (2005), pp. 2390–5. ISSN: 0027-8424.

[32] Ravi A Desai, Natalia M Rodriguez and Christopher S Chen. « Stamp-off" to micropattern sparse, multicomponent features. » In: *Methods in Cell Biology* 119 (2014), pp. 3–16. ISSN: 0091-679X.

[33] Xue Jiang et al. « Cell Growth in Response to Mechanical Stiffness is Affected by Neuron- Astroglia Interactions ». In: *The Open Neuroscience Journal* 1.1 (2007), pp. 7–14. ISSN: 1874-0820.

[34] Thomas Grevesse et al. « Opposite rheological properties of neuronal microcompartments predict axonal vulnerability in brain injury ». In: *Scientific Reports* 5 (2015), p. 9475.

[35] H. Hillborg et al. « Crosslinked polydimethylsiloxane exposed to oxygen plasma studied by neutron reflectometry and other surface specific techniques ». In: *Polymer* 41.18 (2000), pp. 6851–6863. ISSN: 0032-3861.

[36] G. Bar et al. « Investigation of the stiffness change in, the indentation force and the hydrophobic recovery of plasma-oxidized polydimethylsiloxane surfaces by tapping mode atomic force microscopy ». In: *Polymer* 42.8 (2001), pp. 3627–3632. ISSN: 0032-3861.

[37] Peter D Yurchenco and Bruce L Patton. « Developmental and patho-genic mechanisms of basement membrane assembly. » In: *Curr. Pharm. Des.* 15.12 (2009), pp. 1277–94. ISSN: 1381-6128.

[38] Ranjay Jayadev and David Sherwood. « Basement membranes ». In: *Curr Biol* 27.6 (2017), R207–R211. ISSN: 0960-9822.

[39] Lema F Yousif, Jacopo Russo and Lydia Sorokin. « Laminin isoforms in endothelial and perivascular basement membranes ». In: 7.1 (2013), p. 101110. ISSN: 1933-6918.

[40] Joana Bicker et al. « Blood-brain barrier models and their relevance for a successful development of CNS drug delivery systems. A review ». In: *Eur J Pharm Biopharm* 87.3 (2014), pp. 409–432. ISSN: 0939-6411.

[41] Dongeun Huh et al. « Reconstituting organ-level lung functions on a chip. » In: *Science* 328.5986 (2010), pp. 1662–8. ISSN: 0036-8075.

[42] Akihiro Nishiguchi et al. « Basement Membrane Mimics of Biofunctionalized Nanofibers for a Bipolar-Cultured Human Primary Alveolar-Capillary Barrier Model. » In: *Biomacromolecules* 18.3 (2017), pp. 719–727. ISSN: 1525-7797.

[43] Ethan A Winkler, Robert D Bell and Berislav V Zlokovic. « Central nervous system pericytes in health and disease ». In: *Nature Neuroscience* 14.11 (2011), pp. 1398–1405. ISSN: 1097-6256.

[44] Joseph Candiello et al. « Biomechanical properties of native basement membranes ». In: 274.11 (2007), pp. 2897–2908. ISSN: 1742-4658.

[45] Joseph Candiello, Gregory Cole and Willi Halfter. « Age-dependent changes in the structure, composition and biophysical properties of a human basement membrane ». In: *Matrix Biol* 29.5 (2010), pp. 402–410. ISSN: 0945-053X.

[46] Fabian Brau et al. « Multiple-length-scale elastic instability mimics parametric resonance of nonlinear oscillators ». In: *Nat Phys* 7.1 (2010), pp. 56–60. ISSN: 1745-2473.

[47] Jeong Lee et al. « A simple fabrication process for stepwise gradient wrinkle pattern with spatially-controlled wavelength based on sequential oxygen plasma treatment ». In: *Microelectron Eng* 176 (2017), pp. 101–105. ISSN: 0167-9317.

[48] Ned Bowden et al. « The controlled formation of ordered, sinusoidal structures by plasma oxidation of an elastomeric polymer ». In: *Appl Phys Lett* 75.17 (1999), pp. 2557–2559. ISSN: 0003-6951.

[49] Takayuki Okamoto et al. « Gap junction-mediated regulation of endothelial cellular stiffness ». In: *Sci Reports* 7.1 (2017), p. 6134. ISSN: 2045-2322.

[50] Zhongkui Hong et al. « Vascular Smooth Muscle Cell Stiffness and Adhesion to Collagen I Modified by Vasoactive Agonists ». In: *Plos One* 10.3 (2015), e0119533.

[51] Nick Glass et al. « Organosilane deposition for microfluidic applications. » In: *Biomicrofluidics* 5.3 (2011), pp. 36501–365017. ISSN: 1932-1058.

BIBLIOGRAPHY